

# A VORTEX LATTICE PROGRAM FOR STEADY STATE AERODYNAMIC ANALYSIS OF FLAPPED AND TWISTED UAV WING PLANFORMS

Maurício Vicente Donadon, [donadon@ita.br](mailto:donadon@ita.br)

Sérgio Frascino Muller de Almeida, [frascino@ita.br](mailto:frascino@ita.br)

Instituto Tecnológico de Aeronáutica-ITA

CTA-ITA-IEM, Praça Mal. Eduardo Gomes, 50, 12228-900, São José dos Campos-SP, Brazil

Lorenzo Iannucci, [lo.iannucci@imperial.ac.uk](mailto:lo.iannucci@imperial.ac.uk)

Imperial College London, Dept. of Aeronautics, London-UK

## Abstract.

*This paper presents a MATLAB program for estimating the subsonic aero-dynamic characteristics of flapped and twisted wing planforms using the Vortex Lattice Method (VLM). The aerodynamic characteristics of interest are lift, rolling moment, pitching moments about the twisting and flapped line, pressure distribution and aerodynamic energy. The program was developed to help designers to carry out virtual tests in order to decide the wing dimensions for different morphing wing configurations under steady subsonic flow. Numerical results for flat, flapped and twisted wing configurations are presented and discussed.*

**Keywords:** Aerodynamics, Vortex Lattice Method, UAV

## 1. INTRODUCTION

The desire for multi-mission capability in military and civil air vehicle systems has created a need for technologies that allow for drastic wing shape changes during flight. Since most current aircraft are fixed-geometry, they represent a design compromise between conflicting performance requirements in mission segments such as highspeed cruise, low-speed loiter, and low turn radius maneuver. If a hybrid aircraft is designed to combine several flight profiles, the wing design must maximize overall efficiency of the anticipated mission. Through morphing, the aerodynamics of the aircraft can be adapted to optimize performance in each segment by changing areas such as the camber of the airfoils and the twist distribution along the wing. Adapting the shape of wings in flight allows an air vehicle to perform multiple, radically different tasks by dynamically varying its flight envelope. The wing can be adapted to different mission segments, such as cruise, loitering, and high-speed maneuvering by sweeping, twisting, and changing its span, area, and airfoil shape. Within this context, morphing wing technology is considered to be a key component in next-generation unmanned aeronautical vehicles (UAVs) for military and civil application. The design of UAVs and its multidisciplinary nature demands integration of different engineering areas as schematically shown in Fig.1.

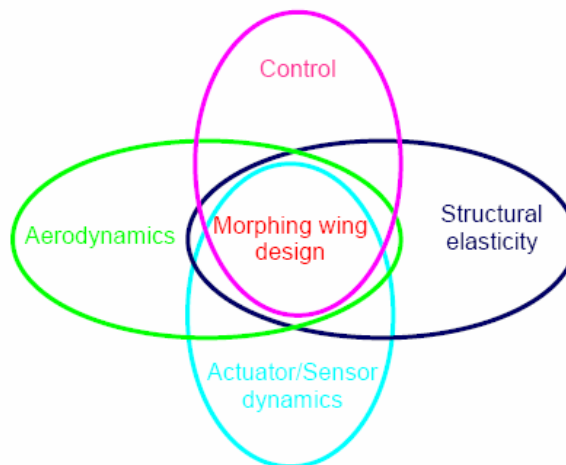


Figure 1. UAV design methodology

One of the crucial and fundamental steps to design UAVs structures is the determination of the aerodynamic loads associated with a given morphing wing configuration. For this purpose, a vortex lattice based program has been developed and presented in this paper. The program enables the prediction of lift, pitching moments, rolling moment and pressure distribution for flat, flapped and twisted wing planforms. Sample cases for flat, flapped and twisted wing configurations are presented and discussed.

## 2. VORTEX LATTICE METHOD (VLM)

As discussed in the previous section, the first step required to solve the aeroelastic problem is the determination of the aerodynamic loads. In order to do so, we have developed a computational program based on the Vortex Lattice Method (VLM) (Donadon and Iannucci, 2006). This section presents a short review on the VLM method and the fundamental equations used in the numerical implementation. The VLM method is the simplest of the methods to solve incompressible flows around wings of finite span (Bertin, 1989). The method represents the wing as a planar surface on which grids of horseshoe vortex are superimposed. The computation of the velocities induced by each horseshoe vortex at each specified control point is based on the Biot-Savart Law (Bertin, 1989). A summation is performed for all control points on the wing to produce a set of linear system of equations for the horseshoe vortex strengths that satisfy the boundary conditions of no flow through the wing. The control points of each element (or lattice) are located at three-fourth of the element's chord and the vortex strengths are related to the wing circulation and the pressure difference between the upper and lower surface of the wing. The pressure differentials are then integrated to yield the total forces and moments. In the approach used here to solve the governing equations, the continuous distribution of bound vorticity over the wing surface is approximated by a finite number of discrete horseshoe vortices, as shown in Fig. 2. The individual horseshoe vortices are placed in rectangular (or trapezoidal) panels also called finite elements or lattices. This procedure for obtaining a numerical solution for the flow is termed Vortex Lattice Method. The bound vortex coincides with quarter-chord line of the element and is therefore, aligned with the local sweepback angle. In a rigorous theoretical analysis, the vortex lattice panels are located on the mean chamber of the wing and, when the trailing vortices leave the wing, they follow a curved path. However, for many engineering applications, suitable accuracy can be obtained linearized theory in which straight line vortices extend downstream to infinity.

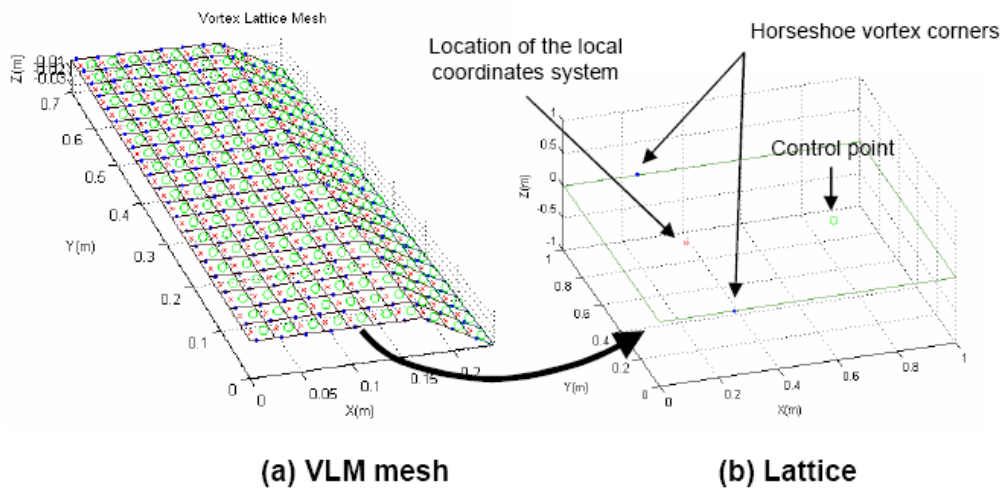


Figure 2. Vortex Lattice discretisation

In the linearized theory the trailing vortices are aligned either parallel to the free stream or parallel to the vehicle axis. Both orientations provide similar accuracy within the assumptions of linearized theory (Bertin, 1989).

### 2.1. Velocity induced by a general horseshoe vortex

Lets assume a typical three dimensional horseshoe vortex composed by a bound vortex segment and two trailing vortex segments as shown in Fig. 3,

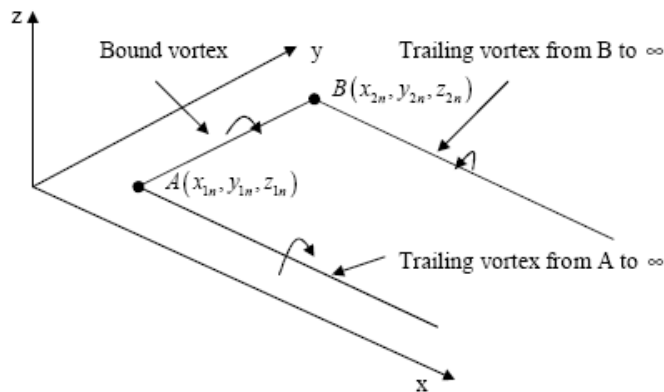


Figure 3. Typical horseshoe vortex

The computation of the velocity induced at some point C(x,y,z) by a vortex segment AB for instance (See Fig.4) is based on the Biot and Savart law as follows (Bertin, 1989),

$$\vec{V}_{AB} = \frac{\Gamma_n \vec{r}_1 \times \vec{r}_2}{4\pi |\vec{r}_1 \times \vec{r}_2|^2} \left[ \vec{r}_0 \cdot \left( \frac{\vec{r}_1}{r_1} - \frac{\vec{r}_2}{r_2} \right) \right] \quad (1)$$

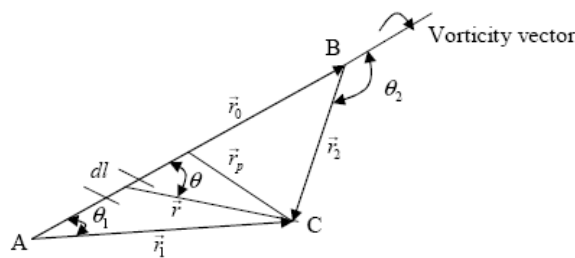


Figure 4. Vortex segment AB

To calculate the velocity induced by the filament that extends from A to  $\infty$ , let us first calculate the velocity induced by the collinear, finite-length filament that extends from A to D according to Fig. 5.

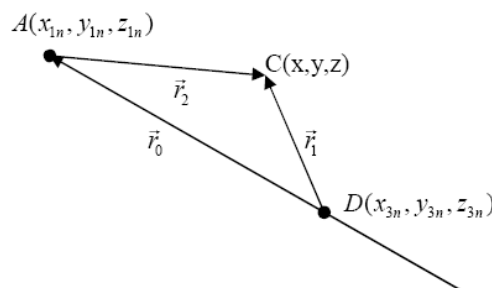


Figure 5. Vortex segment A $\infty$

Applying again Biot and Savart law one can show that the velocity induced by the filament that extends from A to  $\infty$  is given by,

$$\vec{V}_{A\infty} = \frac{\Gamma_n}{4\pi} \left\{ \frac{(z - z_{1n})j + (y_{1n} - y)k}{(z - z_{1n})^2 + (y_{1n} - y)^2} \right\} \left[ 1 + \frac{x - x_{1n}}{\sqrt{(x - x_{1n})^2 + (y - y_{1n})^2 + (z - z_{1n})^2}} \right] \quad (2)$$

Similarly, the velocity induced by the vortex filament that extends from B to  $\infty$  is written as,

$$\vec{V}_{B\infty} = \frac{\Gamma_n}{4\pi} \left\{ \frac{(z - z_{2n})j + (y_{2n} - y)k}{(z - z_{2n})^2 + (y_{2n} - y)^2} \right\} \left[ 1 + \frac{x - x_{2n}}{\sqrt{(x - x_{2n})^2 + (y - y_{2n})^2 + (z - z_{2n})^2}} \right] \quad (3)$$

The total velocity induced at some point (x,y,z) by the horseshoe vortex representing one of the surface elements with trailing vortices parallel to x-axis is

$$\vec{V} = \vec{V}_{AB} + \vec{V}_{A\infty} + \vec{V}_{B\infty} \quad (4)$$

where the total velocity is the sum of the contributions from the three vortex segments shown in Fig.3. Assuming the point  $C(x,y,z)$  to be the control point of the  $m_{th}$  panel, with coordinates  $(x_m, y_m, z_m)$  located at midspan of the element and three-fourth of the elemental chord, we can express the velocity induced at the  $m_{th}$  control point by the vortex representing the  $n_{th}$  panel as,

$$\vec{V}_{m,n} = \vec{C}_{m,n} \Gamma_n = (C_{m,n}^u i + C_{m,n}^v j + C_{m,n}^w k) \Gamma_n \quad (5)$$

where the influence coefficient  $\vec{C}_{m,n}$  depends on the geometry of the  $n_{th}$  panel and its distance from the control point of the  $m_{th}$  panel. Since the governing equation is linear, the velocities induced by the  $2N$  vortices are added together to obtain an expression for the total induced velocity at the  $m_{th}$  control point:

$$\vec{V}_m = \vec{C}_{m,n} \Gamma_n = \sum_{n=1}^{2N} (C_{m,n}^u i + C_{m,n}^v j + C_{m,n}^w k) \Gamma_n \quad (6)$$

## 2.2. Computation of the vortex strengths

To compute the strengths of the vortices,  $\Gamma_n$ , which represent the lifting flow field of the wing, we use the boundary condition that the surface is a streamline. That is, the resultant flow is tangent to the wing at each and every control point. If the flow is tangent to the wing, the component of the induced velocity normal to the wing at the control point balances the normal component of the free-stream velocity. By doing that we can obtain the vortex strengths solving the following linear system of equations (Bertin, 1989),

$$\{\Gamma_n\} = [\vec{C}_{m,n}^w - \vec{C}_{m,n}^v \tan(\phi)]^{-1} 4\pi U_\infty \{\alpha_m\} \quad (7)$$

where  $U_\infty$ ,  $\phi$  and  $\alpha_m$  are the flow velocity, wing dihedral angle and elemental local angle of attack at the  $m_{th}$  control point. The derivation of the elemental local angle of attack is based on Fig.6 and is given by

$$\alpha_m = \text{acos} \left( \frac{\vec{U} \cdot (\vec{p}_1 \times \vec{p}_2)}{|\vec{U}| |\vec{p}_1 \times \vec{p}_2|} \right) - \frac{\pi}{2} \quad (8)$$

with  $\vec{U} = U_\infty \cos(\alpha_i) i + U_\infty \sin(\alpha_i) j$  where  $\alpha_i$  is the angle of attack associated with the incident flow in the plane x - z.

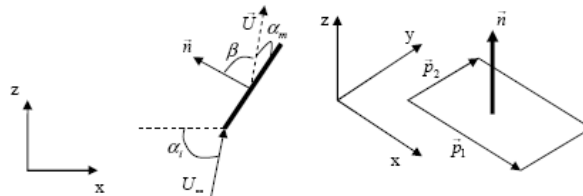


Figure 6. Elemental angle of attack

### 2.3. Lift computation

Having determined the strength of each of the vortices, the lift of the wing may be calculated. The expression to compute the local lift acting on the  $n_{th}$  panel of a wing with no dihedral is given by (Bertin, 1989),

$$\Delta l_n = l = \rho_\infty U_\infty \Gamma_n \quad (9)$$

which is also the lift per unit of span. The total lift of a wing subjected to a symmetric flow is

$$L = 2\rho_\infty U_\infty \sum_{n=1}^N \Gamma_n \Delta y_n \quad (10)$$

where  $N$  is the number of panels of half-wing,  $\Delta y_n$  is the elemental span length and  $\rho_\infty$  is the air density.

### 2.4. Lift coefficient calculation

The expression for the lift coefficient is given by

$$C_L = \frac{L}{q_\infty S_{ref}} = \frac{4}{S_{ref}} \sum_{n=1}^N \frac{\Gamma_n \Delta y_n}{U_\infty} \quad (11)$$

with  $q_\infty = (1/2)\rho_\infty U_\infty^2$  and  $S_{ref} = 0.5s_l(c_r - c_t)$ , where  $s_l$ ,  $c_r$  and  $c_t$  are the wing's semispan length, wing's root chord and wing's tip chord, respectively.

### 2.5. Pitching moments calculation

The formulation presented here enables the computation of pitching moments about two reference lines, named leading line and flapping line (if the wing is flapped) or twisting line (if the wing is twisted). The position of these lines within the mesh is specified by the user and they are shown in Fig.7. The calculation of the pitching moments about the flapping or twisting lines is a fundamental step in the design process because it allows optimisation studies to be carried out for different morphing wing configurations. It also helps in the choice of candidate materials for the deformable parts of the morphing wing enabling the computation power required to achieve a given morphing level. For both flapped and twisted wings the pitching moment about the leading line is given by

$$M_y = 2\rho_\infty U_\infty \sum_{n=1}^N \Gamma_n \Delta y_n x_n^b \quad (12)$$

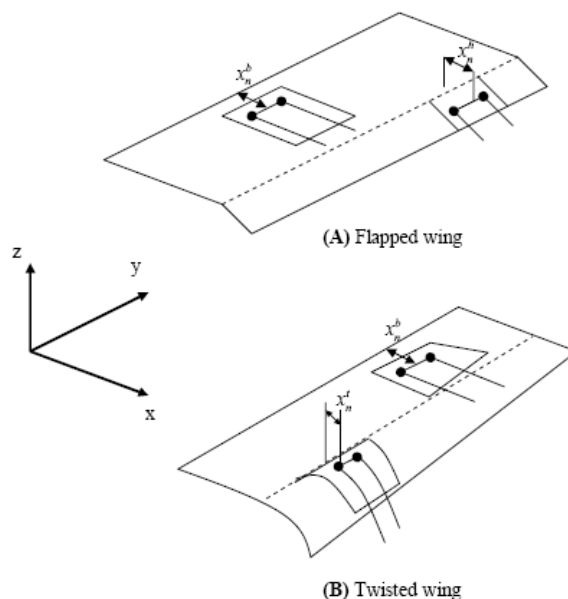


Figure 7. Reference points for pitching moment calculation

where  $x_n^b$  is the distance between the bound vortex filament of each element and the leading line reference, as shown in Fig.7. For flapped wing the pitching moment about the hinge line (or flapping line) is

$$M_y^h = 2\rho_\infty U_\infty \sum_{n=1}^N \Gamma_n \Delta y_n x_n^h \quad (13)$$

where only the lift contributions of the elements ahead of hinge line is considered. In a similar way the pitching moment about the twisting line is given by

$$M_y^t = 2\rho_\infty U_\infty \sum_{n=1}^N \Gamma_n \Delta y_n x_n^t \quad (14)$$

where again only the lift contributions of the elements ahead of the twisting line are considered in the calculation.

## 2.6. Rolling moment calculation

The rolling moment about X-axis of a semi-wing is computed by summing the lift contributions of each strip of elements along the semi-span direction multiplied by the distance of the elemental control points from the root chord as shown in Fig.8,

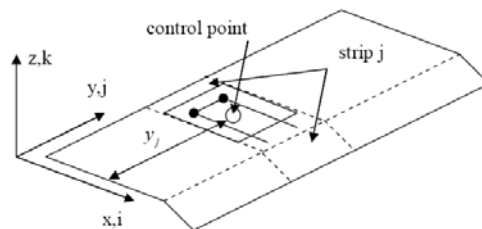


Figure 8. Computation of total rolling moment

$$M_x = \sum_{j=1}^{j_{max}} \left( \sum_{i=1}^{i_{max}} \rho_\infty U_\infty \Gamma_i \right) y_j \quad (15)$$

where  $i_{max}$  and  $j_{max}$  are the maximum number of elements in the chordwise and spanwise directions, respectively.

## 2.7. Moment coefficients calculation

The expressions for the pitching moment coefficients about the leading line, flapping line and twisting line are respectively,

$$C_m = \frac{M_y}{q_\infty S_{ref} c_{ref}} \quad (16)$$

$$C_m^h = \frac{M_y^h}{q_\infty S_{ref} c_{ref}} \quad (17)$$

$$C_m^t = \frac{M_y^t}{q_\infty S_{ref} c_{ref}} \quad (18)$$

with  $c_{ref} = 0.5(c_{root} + c_{tip})$ , where  $c_{root}$  and  $c_{tip}$  are the root chord and tip chord dimensions, respectively.

## 2.8. Incremental pressure coefficient calculation

The incremental pressure coefficient for the  $n$ -th element is given by (Margason, 1971),

$$\Delta C_{p,n} = \frac{2\Gamma_n}{c_n U_\infty} \quad (19)$$

where  $c_n$  is the elemental chord.

## 2.9. Aerodynamic energy calculation

The term aerodynamic energy defined here refers to the total energy generated by the total moments acting on the deformable parts of the wing only. For a flapped wing the expression for aerodynamic energy is given by

$$W_h = \int_0^{\theta_f} M_y^h(\theta) d\theta \quad (20)$$

where  $\theta$  is the flap deflection. In a similar way the aerodynamic energy for twisted wings is written as

$$W_t = \int_0^{\phi_f} M_y^t(\phi) d\phi \quad (21)$$

where  $\phi$  is the maximum twisting angle at the tip of the wing.

## 3. NUMERICAL SIMULATIONS

Numerical simulations for flapped and twisted wings have been carried out using the methodology and the program proposed in this paper. A direct comparison in terms of lift distribution, pressure distribution and aerodynamic energy for both wing configurations is also presented and discussed.

### 3.1. Flapped wing

The dimensions as well as flight conditions for the flapped wing simulated here are typical of small UAV's and they are listed in Tables 1 and 2, respectively.

Table 1. Flapped wing dimensions

Span Length (m)	1.40
Root chord (m)	0.27
Tip chord (m)	0.27
Angle of attack (Degrees)	3.0
Flap deflection (Degrees)	10.0

Table 2. Flight conditions and air properties

$U_\infty$ (m/s)	Altitude (m)	$\rho_\infty$ (kg/m <sup>3</sup> )
40.0	1000	1.117

The flapping line was positioned at 70% of the chord and the flap deflection was assumed to be  $10^\circ$ . It was found that a mesh density of 20 elements spanwise by 10 elements chordwise gives results within an accuracy of less than 1% compared to more refined meshes and for this reason this mesh density was used for all simulations presented in this section. A typical Vortex Lattice (VL) mesh for the flapped wing obtained using the pre-processor module is shown in Fig.9.

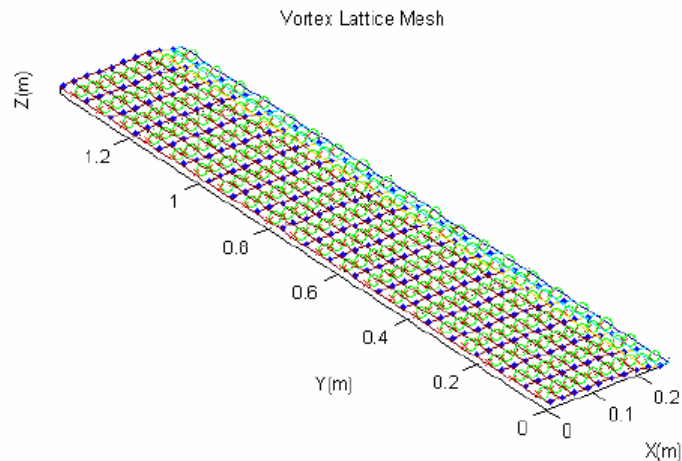


Figure 9. VL mesh for the flapped wing

It is well known that flat planforms exhibits a parabolic lift distribution along the spanwise direction with a smooth lift decay along the chordwise direction, with maximum lift close to the leading edge and minimum lift in regions near by the trailing edge for angles of attack different from zero. As an initial assessment, the flap deflection was assumed to be zero in order to verify such a behaviour and the lift distribution fringe as well as the 3D lift plotting representation for a flat wing without flaps with dimensions given in Tab.1 are shown in Fig. 10. The results shown in Fig. 10 agree very well with results reported elsewhere (Bertin, 1989), for similar planforms.

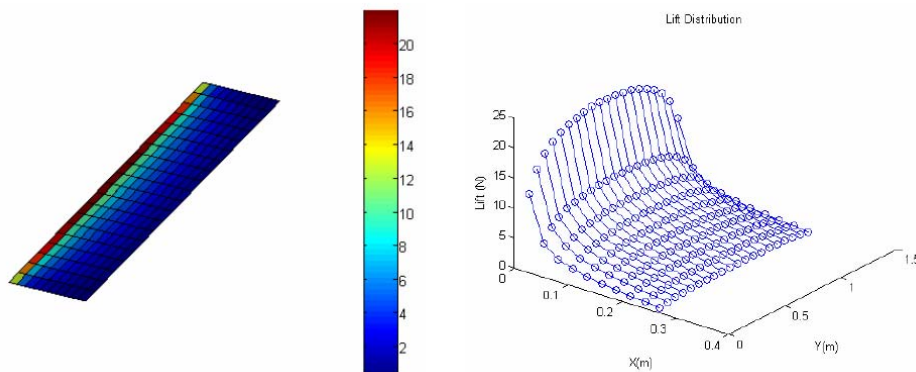


Figure 10. Lift distribution for flat wing

Fig.11 shows the numerical results in terms of lift and pressure distributions for a flapped wing with with dimensions shown in Tab.1 under flight conditions presented in Tab.2. It can be seen from Fig.11 that there is a singularity in both lift and pressure distributions around the flapping line. This singularity is due to the change in the local angle of attack which increases the vorticity strength in this region affecting both lift and pressure distribution. The numerical results indicated that the lift generated by the flapped wing is higher (about three times higher) than the lift generated by the flat one, as expected. A similar trend was also observed for the pitching moments coefficients about the leading edge, with  $C_m=0.55$  for flapped wing and  $C_m=0.10$  for flat wing. It was also noticed a significant increase in the pitching moments about the flapping line for the flapped wing compared with the flat one due to the higher vorticity strength in the flapped region of the wing, which increases the pressure in that region. The results presented here agree with experimental and numerical data reported in the open literature (Margason, 1971).

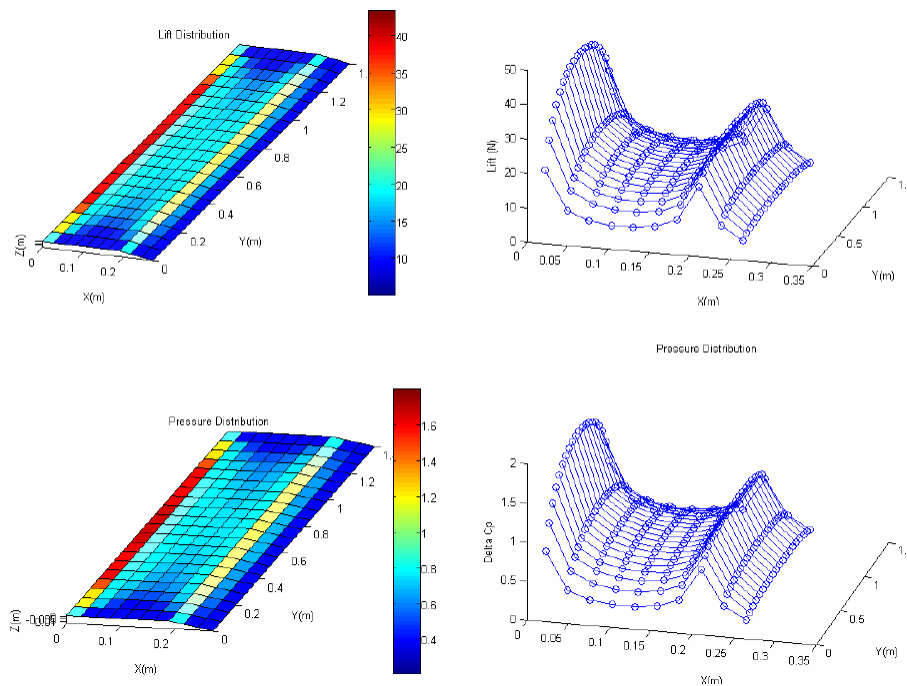


Figure 11. Lift and pressure distributions for flapped wing

### 3.2. Twisted wing

The dimensions of the twisted wing were essentially the same as the ones defined for the flapped wing in order to provide a direct comparison between both wing planforms in terms of lift, pitching moments and aerodynamic energy generation. The flight conditions for the twisted wing were also assumed to be the same as those defined in Tab.2. The twisted wing dimensions together with the wing's tip deflection are presented in Tab.3. The twisting line was placed along the leading edge extending in the spanwise direction from initial coordinates  $(x_i, y_i) = (0, 0)$  up to the wing's tip. The VL mesh for the twisted wing is shown in Fig.12 and the lift and pressure distributions for the twisted wing are shown in Fig.13.

Table 3. Twisted wing dimensions

Span Length (m)	1.40
Root chord (m)	0.27
Tip chord (m)	0.27
Angle of attack (Degrees)	3.0
Twisting angle at wing's tip (Degrees)	10.0

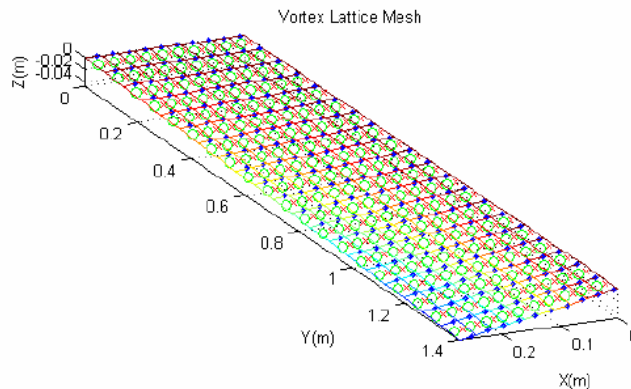


Figure 12. VL mesh for the twisted wing

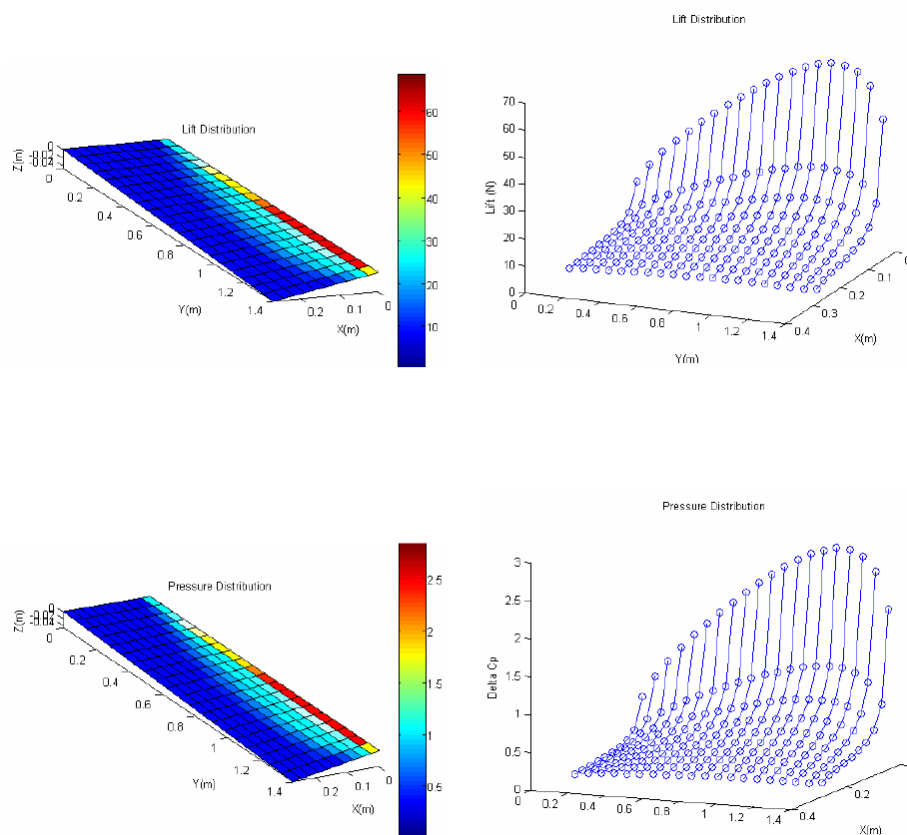


Figure 13. Lift and pressure distributions for the twisted wing

#### 4. CONCLUSIONS

This paper presented a detailed formulation of the Vortex Lattice Method (VLM) for both flapped and twisted wing planforms. The proposed formulation has been implemented into MATLAB software and an user interface with pre-processor, solver and post-processor capabilities was developed to help designers to design morphing wing structures. A detailed description of the numerical implementation was also presented and discussed. Numerical simulations were carried out for a typical small UAV considering two morphing concepts: flapped and twisted wing configurations. The numerical results indicated that the flapped wings generated higher lift compared to the twisted one for the same deflection range. Furthermore, less aerodynamic power was required to sustain the flapped wing against the aerodynamic loads compared to the twisted wing configuration. These findings indicated that flapped wing configurations have a better aerodynamic performance compared to the twisted wings, however, there is still a need of further investigation considering local twisting instead of twisting the whole wing. This can be easily achieved by just changing the coordinates of the twisting line in the pre-processor. A better aerodynamic performance means that the deformable parts of the wing can be made of lighter smart materials with lower specific energy which allows the fabrication of lighter aircrafts with higher performance and less fuel consumption.

#### 5. ACKNOWLEDGEMENTS

The authors acknowledge the financial support received for this work from British Aerospace UK, Fundação de Amparo Pesquisa do Estado de São Paulo (Fapesp), contract numbers 2006/06808-6, 2007/02710-4 and CNPq Grant 305601/2007-5.

#### 6. REFERENCES

- Bertin J. J., 1989, Aerodynamics for Engineers, Prentice-Hall Inc., 2nd ed.
- Donadon M. and Iannucci L., 2006, "A vortex lattice program to compute aerodynamic loads in flapped and twisted wing planforms," Flaviir project-Internal report, Imperial College London-UK.
- E. L. J., 1976, "A vortex-lattice method for the mean camber shapes of trimmed noncoplanar planforms with minimum drag," NASA TN D-8090.

Margason J. R., 1971, "Vortex-lattice fortran program for estimating subsonic aerodynamic characteristics of complex planforms," NASA TN D-6142.

## **7. RESPONSIBILITY NOTICE**

The authors are the only responsible for the material included in this paper.